

# Computations of bladerow stall inception in transonic flows

L. He

School of Engineering

University of Durham, Durham, UK

J. O. Ismael

Department of Engineering Systems

Brunel University, Uxbridge, UK

## ABSTRACT

A three-dimensional unsteady Navier-Stokes solver has been used to simulate stall inception in a single row ten passage segment of a transonic fan, the NASA rotor-67. At subsonic flow conditions, the 3D results illustrate a rotating stall inception with short scale part-span cells rotating at around 80% rotor speed, similar to that observed in some low speed experiments. However, at a supersonic relative inflow condition, the results show that an isolated blade row tends to stall in a one-dimensional breakdown pattern without first experiencing rotating stall. At near-stall conditions, significant self-excited unsteadiness is generated by the interaction between the tip-leakage vortex and the passage shock wave. Further computations for two-dimensional configurations indicate that it is possible to have a rotating pattern of instability in transonic blade rows associated with circumferential synchronised shock oscillation.

## NOMENCLATURE

$k$	constant
$P_{exit}$	exit pressure
$P_{ref}$	reference pressure
$V_x$	mass averaged axial velocity on the exit plane
$\rho_{ref}$	reference density

## 1.0 INTRODUCTION

The performance of axial-flow compressors is ultimately limited by instabilities which lead to flow breakdown at sufficiently high loading levels. The important aerodynamic instabilities are rotating stall and surge. It is now generally understood that rotating stall is the mechanism by which the flow field in compressors will breakdown and leads to surge cycles. There has been a revived interest in this phenomenon directed towards its active control by suppression of stall cells prior to their full development<sup>(1, 2)</sup>.

Conventional methods of modelling rotating stall adopt a lumped parameter approach whereby characteristics of the blade passage flow are supplied to the model<sup>(3)</sup>. While this approach has been successful in computing stall for subsonic flow regimes its

application to transonic regimes remains uncertain. On the other hand, with the aid of modern high performance computers, it is now also possible to directly compute rotating stall for simple configurations (single blade rows and stages). A number of studies of this kind have been reported<sup>(5-7)</sup> which serve to demonstrate the potential utility of CFD in examining stall inception without recourse to much empiricism.

The objective of the present study was to examine stall under transonic conditions by three-dimensional unsteady Navier-Stokes simulations. Now, it is usually found that stable rotating stall occurs at low speeds whereas surge develops at high speeds as a consequence of the high compression energy stored in the exit plenum, as well established in a lumped-parameter system analysis using an essentially incompressible flow model by Greitzer<sup>(4)</sup> (1976). Although the overall characteristics of surge cycles are quite well understood, very little is known about the manner in which the flow initially breaks down at a blade-passage level. It is of considerable importance to identify whether or not rotating stall would be a 'precursor' of surge instability for high-speed situations. In this context, one might ask what would happen in stall inception if a relative inlet flow to blade-passages becomes supersonic.

Here, we seek to address the question of transonic stall inception for the simplest three-dimensional case of an isolated transonic rotor row. A fully 3D stall simulation is presented for a ten passage segment of the well-studied NASA rotor 67 transonic fan<sup>(8)</sup>. The results raise an issue regarding the occurrence of rotating stall in transonic flow regimes which are further explored with reference to two-dimensional single blade row and stage computations.

## 2.0 COMPUTATIONAL MODEL AND METHOD

In the present study the full three-dimensional unsteady Navier-Stokes equations are solved in a stationery cylindrical co-ordinate system<sup>(9,17)</sup>. For turbulent flows, eddy viscosity is determined by the Baldwin-Lomax model<sup>(10)</sup> assuming surface boundary layers to be fully turbulent.

Direct repeating (periodic) boundary conditions are applied at circumferential boundaries of the computational domain containing multiple blade passages. In order to avoid resolution of steep gradients in the region near solid surfaces a slip boundary condition is employed in combination with a zero flux condition. For this type of condition a wall function which assumes a log-law variation of velocity normal to the solid surface is used to determine wall shear stress<sup>(11)</sup>. The code used in the present study implements the 2D non-reflecting boundary conditions developed by Giles<sup>(12)</sup>. Within the framework of these conditions the mean circumferential values of stagnation pressure, temperature and flow angle are set to zero at the inflow. Mean circumferential pressure is set to zero at the exit plane and its spanwise equilibrium.

The governing equations are solved using a second order accurate finite volume method. A standard blend of 2<sup>nd</sup> and 4<sup>th</sup> order artificial dissipation (Shen *et al*<sup>(13)</sup>) is included to stabilise the solution and temporal integration is carried out using a four-step Runge-Kutta algorithm. A great increase in the computational efficiency of the present scheme is achieved by using the two-grid integration technique of He<sup>(14)</sup> at each stage of the Runge-Kutta algorithm. Typically, it is possible to extend CFL numbers by a factor of at least seven for the type of three-dimensional simulation considered here.

Overtip-leakage is modelled simply by applying repeating (periodic) boundary conditions for points on the blade surface residing within the clearance gap.

low-quality numerical simulation

on meridional and blade-to-blade planes: the mesh dimensions are  $86 \times 28 \times 16$  per passage in the axial, pitchwise and spanwise directions respectively. The same mesh density was subsequently used for ten passages stall computations. Preliminary calculations indicated that for this rotor stall would be initiated in the region of the blade tip, thus over the span of the mesh domain nodes are concentrated towards the casing. The clearance gap is 0.8% span, which is spanned by only one mesh cell in the radial direction. An inflow boundary layer is introduced to the casing end wall following the measured variation of stagnation pressure, however, the inflow boundary layer is neglected on the hub end wall where the mesh is clearly incapable of resolving its thickness.

Total pressure and efficiency characteristics for the rotor at its design speed were computed from nine individual runs, each over 4000 time steps after which point little variation was observed in the computed mass flow. Figure 2 compares computed results with data. Here, mass flow is normalised by a predicted choking flow of  $34.5 \text{ kg s}^{-1}$  lying 1.2% below the measured value of  $34.93 \text{ kg s}^{-1}$ . Stable solutions were unobtainable below a mass flow ratio of around 0.91. Evidently, the computed results are in quite close accord with the experimental data, although there is some quantitative error in the level of efficiency, around 1-2% as stall is approached.

Further comparisons with flow data for near-stall and near-peak efficiency conditions are presented in Figs 3 and 4. The two conditions were matched to the measured mass flow ratios of 0.989 and 0.925 for the near-peak-efficiency and near-stall points respectively by trial and error. Nonetheless, from Fig. 3 it is seen that the predicted and measured spanwise distributions of exit pressure, which might be viewed as the externally imposed condition, agree well for the two cases. The remaining graphs in Fig. 3 compare the spanwise distributions of exit angle, total temperature and total pressure downstream of the rotor with data. Clearly, trends in these data are well matched and the absolute level of agreement is also fairly good. Figure 4 compares Mach number contours on a blade-to-blade plane 10% chord from the casing. Here, the overall pattern of the measured

### 3.0 STEADY FLOW VALIDATION

Initially a series of single passage calculations was carried out to validate the solver in computing the steady flow performance of the NASA rotor 67 fan. Figure 1 shows projections of the mesh used (extending over the ten passages calculated for the stall simulation)

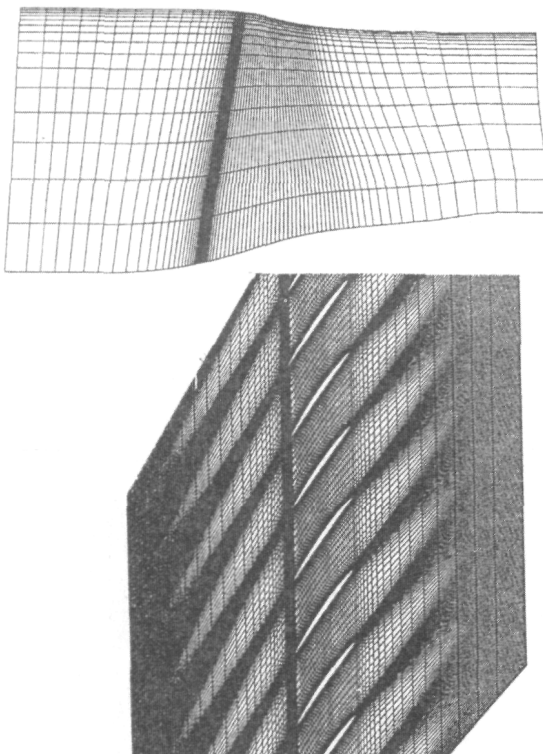


Figure 1. Computational mesh (above: meridional projection, below: blade-to-blade projection).

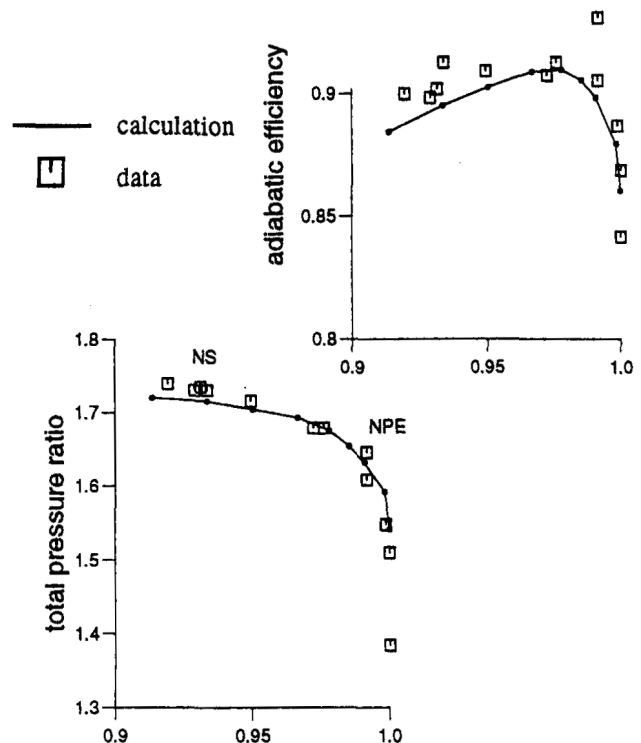


Figure 2. Total pressure and efficiency characteristics. NS-near stall; NPE-near peak efficiency.

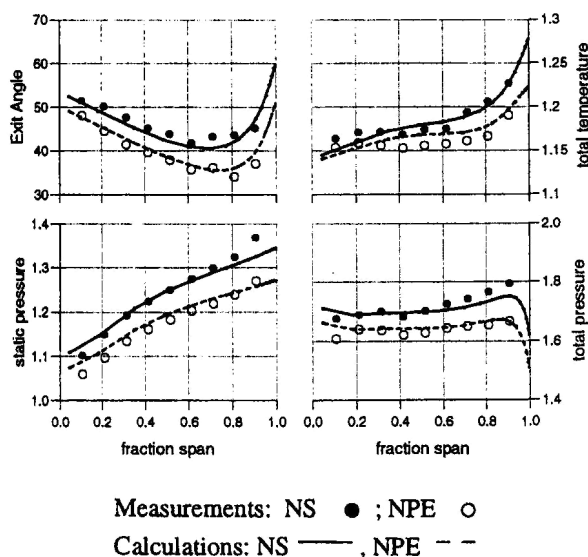


Figure 3. Exit survey data.

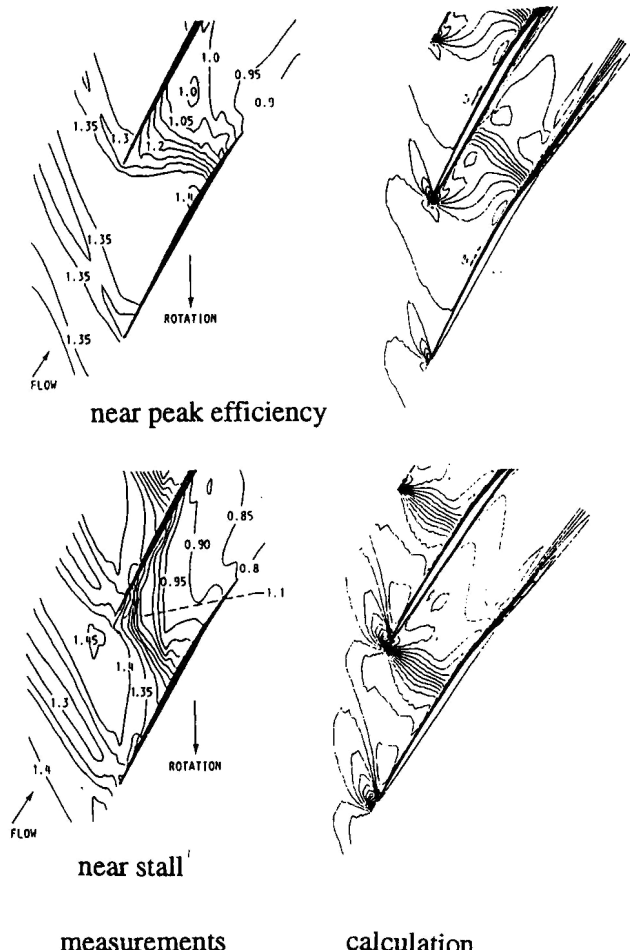


Figure 4. Relative Mach number distributions on plane 10% span from casing.

It will be seen below that numerical results suggest that the clearance flow plays an important role in the development of stall in this rotor. In order to aid the discussion of this effect we shall consider briefly the predicted development of the clearance flow from the near-peak efficiency to near-stall condition. Figure 5 presents Mach number distributions on a blade-to-blade plane through the clearance gap and also the path three-dimensional streamlines within the clearance gap (which more clearly distinguish the path of the clearance vortex). A good description of the structure of the endwall flow for transonic fans is given by Puterbaugh and Brendel<sup>(16)</sup> with which the present computations are in good qualitative agreement. For the peak efficiency condition the clearance flow emerges from the gap with little axial momentum and rolls up into a vortex on meeting the oncoming flow. Downstream of the shock the vortex develops a distinctive low momentum core (visible on the relative mach number plots) which progressively diffuses out with increasing distance upstream of the shock. The pattern of development is similar at the near-stall condition, although in this case the clearance flow emerges more strongly from the region upstream of the shock.

#### 4.0 THREE-DIMENSIONAL SINGLE ROW COMPUTATIONS

Starting from a steady flow solution near stall, the progression to stall has been examined for an isolated row of ten blade passages.

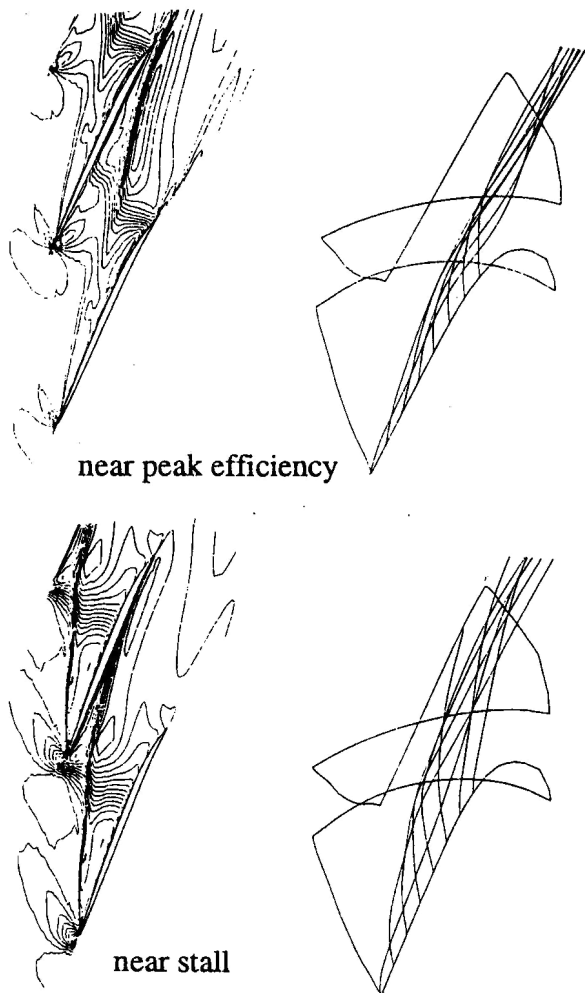


Figure 5. Predicted relative Mach number distribution and streamlines in the region of tip gap.

contour distributions is captured. At the near-peak-efficiency condition the predicted shock position is a little upstream of the measured position, although the predicted shock position is better for the near-stall condition.

#### 4.1 Throttling

As noted above, the circumferential mean value of exit pressure is specified at only one point on the exit plane, 15% span from tip, and the spanwise distribution is continually updated using radial equilibrium. Throttling into stall is then accomplished by increasing this pressure. Although the most direct route to accomplish this throttling would be to prescribe the variation of pressure in, say, a linear fashion<sup>(20)</sup>, in the present computations a simple throttle model is used: exit pressure is made dependent on mean exit velocity as

$$P_{exit} = P_{ref} + kp_{ref}V_x^2 \quad \dots (1)$$

The reference values chosen for pressure and density are the specified inlet stagnation conditions and  $V_x$  is the mass averaged axial velocity on the exit plane. The intention here is that Equation (1) should represent an idealised throttle valve placed between the rotor exit and ambient conditions. The constant  $k$  is increased in order to raise pressure. Here, stall is induced by raising the  $k$  by 5% per 20,000 time steps (corresponding to approximately 16 revolutions of the ten passage rows).

Throughout throttling a small-amplitude-harmonic circumferential distortion of inflow stagnation pressure is applied to simulate external noise. The distortion is fixed in the absolute frame and has an amplitude equal to 5% of the rotor inlet dynamic head. A detailed discussion of the influence of such inflow distortions on two-dimensional stall inception is given by He<sup>(20)</sup>.

#### 4.2 Rotating stall at 50% speed

Let us first briefly examine results at 50% of the rotor design speed. At this speed, for which the flow field around the blades was entirely subsonic, a rotating stall pattern was predicted. Figure 6 shows the time history of axial velocity taken from uniformly spaced circumferential positions 50% chord upstream of the leading-edge and 10% span from tip. A single rotating cell emerges after 16 revolutions which rotates in the absolute frame at 80% rotor speed. Figure 7 shows the development of instantaneous entropy contours on an  $r\theta$  plane at the mid-chord location. It can be seen that the rotating stall cell covers about 30% span in the tip region. The calculated pattern looks like a typical part-span rotating stall cell normally observed experimentally at low speed conditions.

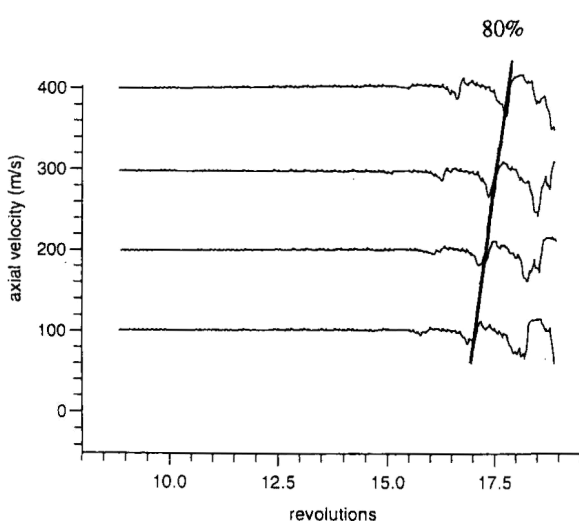


Figure 6. Stall inception at 50% speed. Upstream axial velocity 10% span from casing.

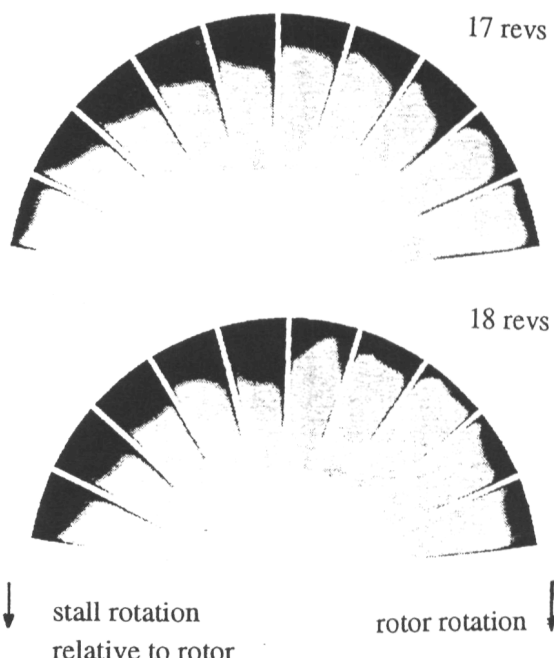


Figure 7. Stall inception at 50% speed. Development of entropy at midchord section.

#### 4.3 Stall at 100% speed

The main interest here is what would happen at the rotor design speed for which the rotor tip velocity is supersonic. The results reveal a distinctly different picture from what is seen at 50% speed. Figure 8 shows the time history of axial velocity upstream of the rotor, 10% span from tip and in this case 15% chord upstream of the rotor, for the design speed. Here, numerical probes register a marked reduction in velocity nearly simultaneously at about 38 rotor revolutions. Figure 9 shows the development of instantaneous Mach number contours on a  $r\theta$  plane at the mid chord section. The predicted behaviour is more characteristic of a one-dimensional 'surge-like' breakdown than of the emergence of a rotating stall cell.

There might be a simple explanation for this behaviour based on consideration of stall in a two-dimensional row. Consider first the case of entirely subsonic flow as illustrated in Fig. 10. Following

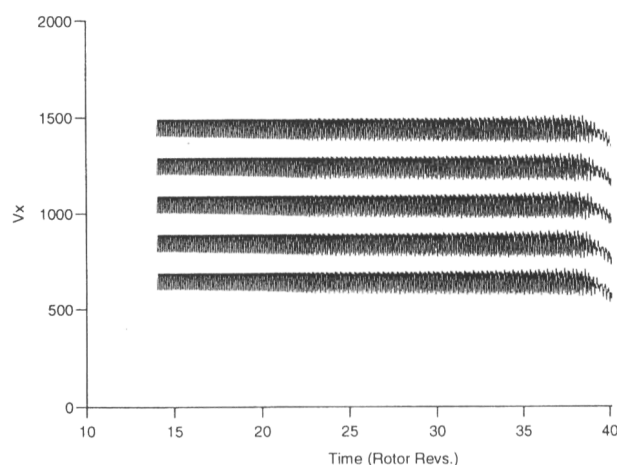


Figure 8. Stall inception at 100% speed. Upstream axial velocity 10% span from casing.

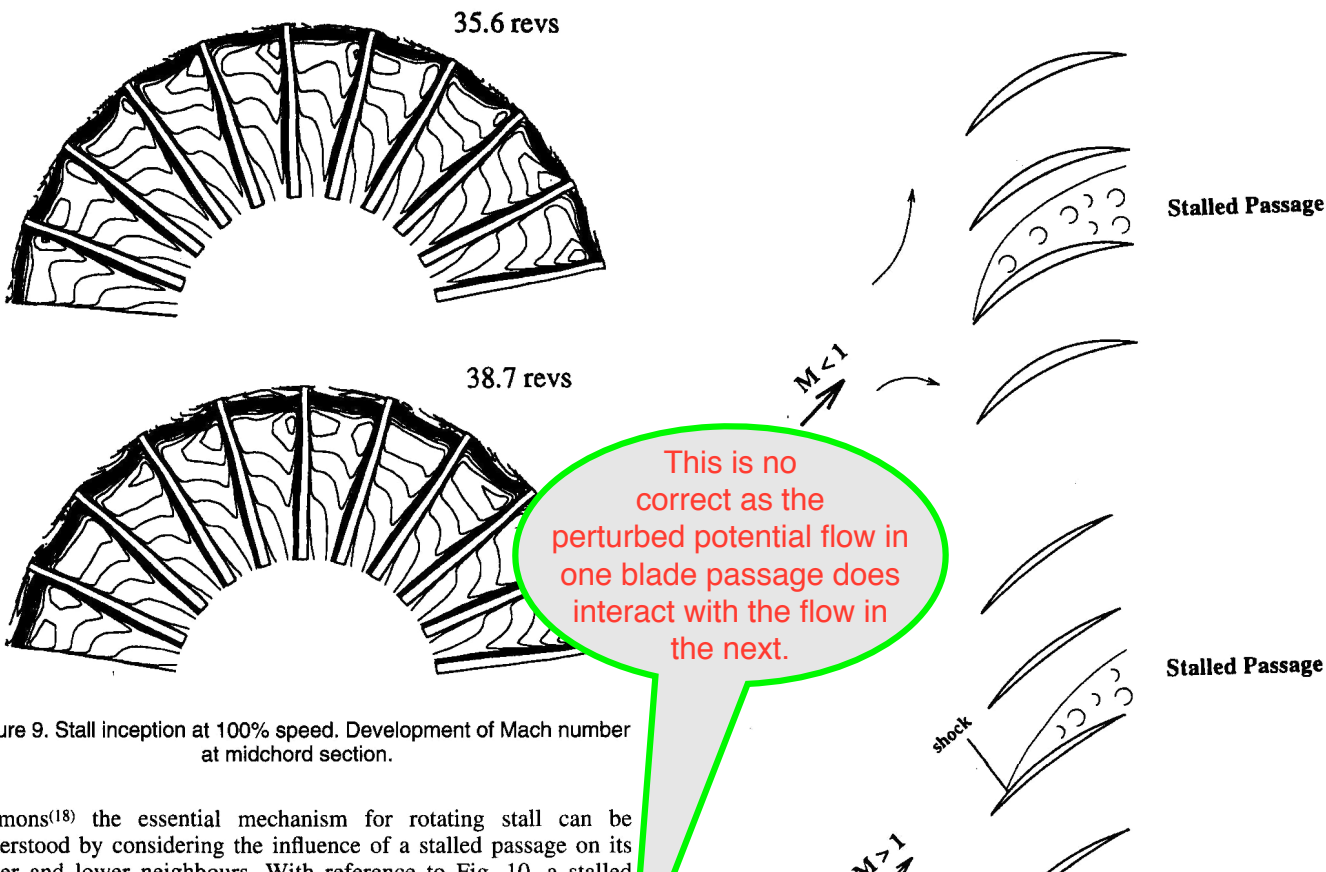


Figure 9. Stall inception at 100% speed. Development of Mach number at midchord section.

Emmons<sup>(18)</sup> the essential mechanism for rotating stall can be understood by considering the influence of a stalled passage on its upper and lower neighbours. With reference to Fig. 10, a stalled passage tends to increase incidence on its upper neighbour thus promoting stall in it, and tends to reduce incidence in its lower neighbour thus relieving it. In this way the stall may rotate in a direction opposite to the direction of blade rotation. Now consider the case of transonic flow illustrated in Fig. 10. Clearly, for this case a stalled passage may not communicate easily with its lower neighbour, so that there seems to be no unstalling mechanism. Consequently a mechanism for cell rotation is much less obvious.

This scenario of rotating stall at lower speeds and the 1D breakdown at higher speeds was, in fact, observed by the present authors in single row computations previously reported<sup>(17)</sup> without tip clearance included. In this earlier work it was found that stall was initiated by spanwise migration of fluid within the suction surface boundary layer. The fluid collected in the endwall region, gradually increasing blockage, until the flow field broke down. A quite different progression to stall is observed for the present simulation where tip clearance is included. In this instance stall occurs as a consequence of breakdown in the tip-leakage flow. Figure 11 shows the development of velocity on numerical probes placed 15% chord upstream of the rotor at three spanwise positions; Fig. 12 traces the development of Mach number on blade-to-blade planes within the clearance gap. Up to 23 rotor revolutions of throttling the pattern of the flow field remains essentially unchanged from the stall condition discussed above. Little difference can be observed in the distributions of Mach number in each of the passages. Now, on further throttling, an oscillatory instability in the endwall flow is predicted which is evident both on the upstream axial velocity traces (Fig. 11) and on the distributions of Mach number (Fig. 12). Here, the loss of axial momentum after the shock appears to be so severe as to cause an unstable separation of the end wall flow. We also observed some oscillation of the shock pattern associated with the instability of the end wall flow although its amplitude does not appear to increase dramatically as eventual breakdown of the flow field is approached. Unstable motion continues to 38 rotor revolutions at which point the flow field is observed to 'surge' forward in a one-dimensional pattern.

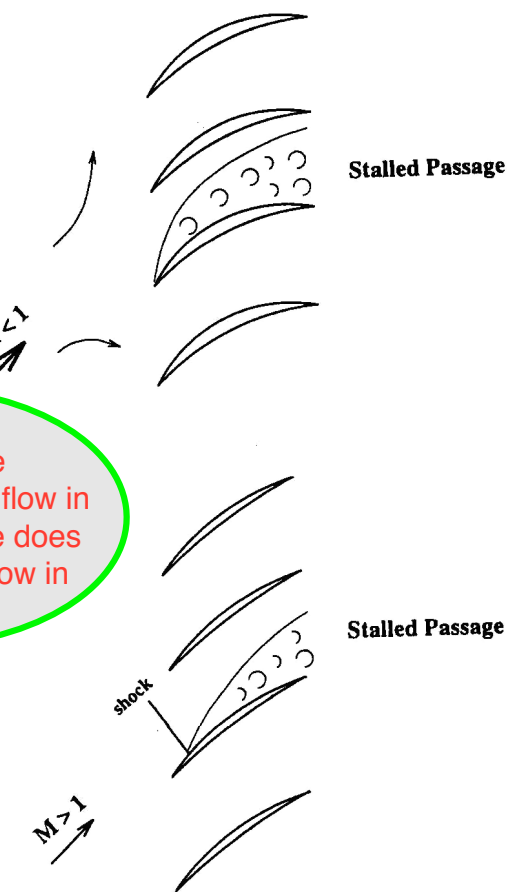


Figure 10. Schematic diagrams of stall inception in subsonic flow (above) and transonic flow (below).

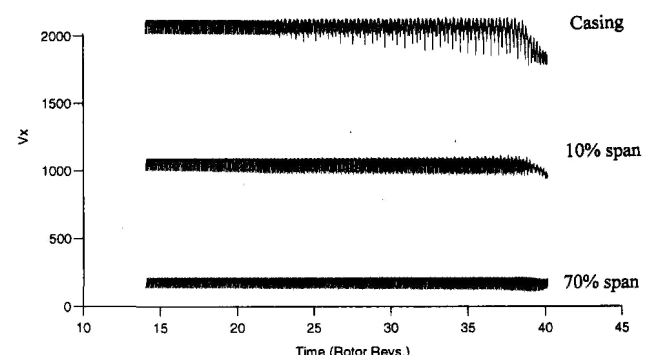


Figure 11. Stall inception at 100% speed. Upstream axial velocity at various spanwise location (measured from the casing).

The tendency to surge directly at a supersonic inlet flow condition is also relevant to practical CFD prediction of instability point. Since the temporal length scale of a surge breakdown is considerably longer than that of rotating stall, it could be argued the 'numerical surge' predicted by single-passage steady flow solvers should be adequate for determining the instability point at a supersonic flow condition.

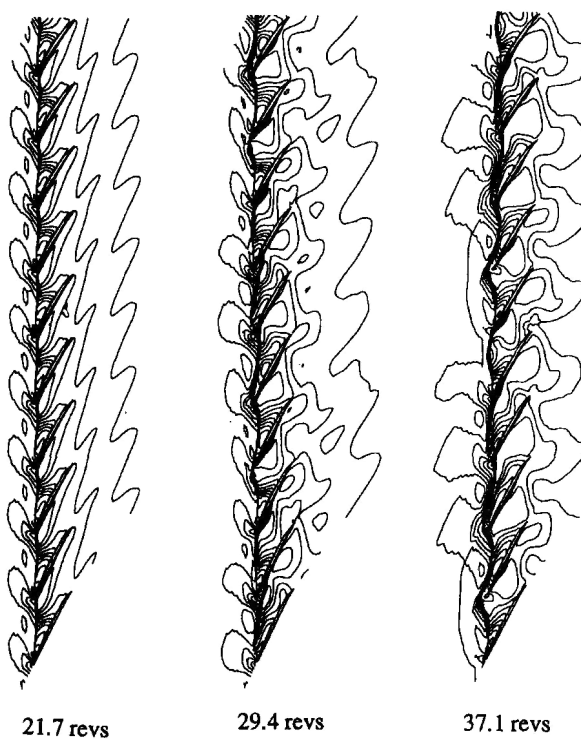


Figure 12. Stall inception at 100% speed. Development of Mach number on blade-to-blade plane in tip gap.

## 5.0 TWO DIMENSIONAL STALL COMPUTATIONS

It is recognised that most methods commonly used for the prediction of rotating stall at low speeds are based on the two-dimensional flow model. The classic Emmons model provides a simple but physically sound mechanism for a rotating stall cell to evolve in a 2D context, notwithstanding the possibility that 3D effects have some role to play in the inception process. This may be the reason why conventional 2D models are able to satisfactorily reproduce rotating stall inception data. However, the results presented above for three dimensional flow raise some questions regarding the validity of the Emmons 2D mechanism under transonic conditions. It seems to be reasonable to ask whether it is possible to generate rotating stall in a 2D transonic cascade? If rotating stall is possible in 2D transonic flows, we might have to look for a mechanism other than that given in the Emmons model.

### 5.1 Rotor-stator stage

Because of the distinctive difference in stall inception between a transonic and a subsonic blade row, it seems worthwhile examining a typical transonic stage in which a transonic rotor row is followed by a subsonic stator row. Here we consider a two-dimensional stage computation. The mesh grids are fixed to rotor and stator blades respectively and a sliding interface is adopted as detailed by He<sup>(20)</sup>. The stage has 20 rotor blades and 21 stator blades.

Stall was generated in this stage configuration by raising the exit pressure gradually from  $P_{exit}/P_{01} = 1.16$  to  $P_{exit}/P_{01} = 1.3$ . The pressure ratio of  $P_{exit}/P_{01} = 1.16$  corresponds to the peak efficiency condition with a stage total-to-total efficiency of 0.9. The relative inlet Mach number at this peak efficiency is about 1.13. Figure 13 shows the time traces from eight axial velocity 'probes', around stall inception. Four of the numerical 'probes' are circumferentially evenly located

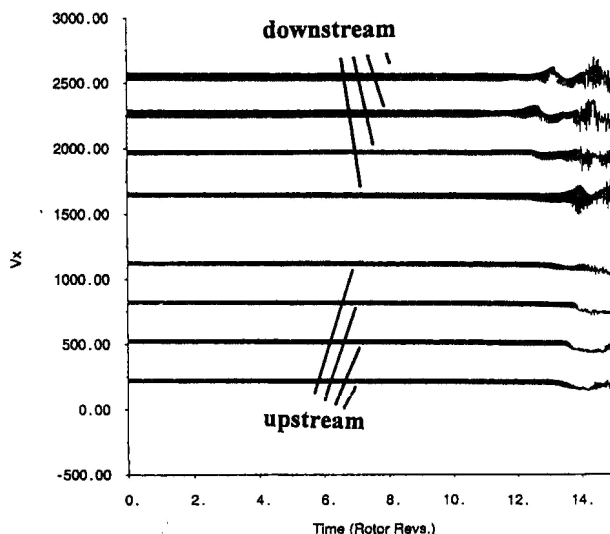


Figure 13. Time-history of axial velocity upstream and downstream of rotor in a transonic stage ( $NB_R = 20$ ,  $NB_S = 21$ ,  $P_{exit}/P_{01} = 1.3$ ).

upstream of the rotor row. The other four are placed in the same manner at a location between the trailing edge of the rotor blades and the leading edge of the stator blades. It is seen that a rotating stall pattern is first detected downstream of the rotor, suggesting that the stator row goes into rotating stall first. Figure 14 shows instantaneous absolute Mach number contours after the rotating stall is initiated. The stator row is apparently subject to a rotating stall pattern with some of its passages being almost filled with separated flows. On the other hand, the circumferential rotating pattern in the rotor is associated

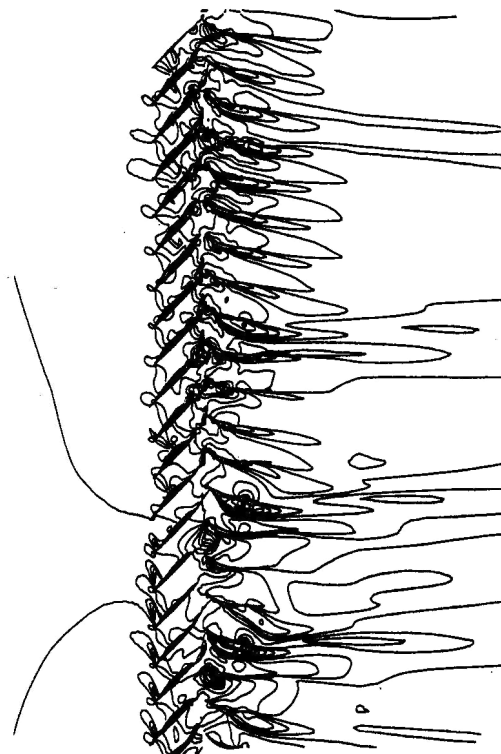


Figure 14. Instantaneous absolute Mach number contour for a transonic stage after stall inception.

with large scale shock wave movement in the rotor blade passages. These results suggest that rotating stall is in fact initiated in the subsonic stator row. The stalled pattern in the transonic rotor row seems to be driven to rotate.

## 5.2 Isolated rotor row

A calculation was then carried out for the rotor in isolation under the same inlet flow condition as in the stage calculation. In this case, a circumferential nonuniformity in static pressure was introduced at the exit. The disturbance is in the 1<sup>st</sup> harmonic form fixed in the absolute frame with an amplitude of 2% of the mean static pressure at the exit. As the mean exit pressure was gradually increased, a rapid drop in performance (stagnation pressure ratio and mass flow) was observed. Figure 15 shows the time traces of the axial velocities upstream and downstream of the rotor around the performance breakdown condition. It can be seen that in the time between two rotor revolutions and six revolutions, the mean upstream axial velocity drops by about 30%. In the same time, the downstream velocities become very unsteady. It is noteworthy that the upstream velocity probes clearly indicate a rotating pattern during this period of performance breakdown. The rotating speed of the pattern is about 75% of the rotor speed, similar to that of a typical short-scale rotating stall cell observed at low speed conditions. Figure 16 shows the instantaneous Mach number contour plots at four instants in one rotor revolution. The figure clearly illustrates that a synchronised oscillatory shock structure travelling circumferentially at a relative speed of about 25% rotor speed. It should also be noted that this 'rotating-stall-like' shock oscillation pattern is very transitional. After about three rotor revolutions from the inception of shock oscillation, the pattern almost completely disappears. The flow in rotor passages then becomes deeply stalled as is shown in Fig. 17. Apparently, the separated flow pattern cannot sustain itself in the rotor passages and large separated vortical flow structures are shed from the blades. The shedding of these structures seems to be mainly random resulting in the marked velocity fluctuations on the four downstream axial velocity traces (Fig. 15). In spite of the large unsteadiness due to the shedding of separated vortical flow structures, the deeply stalled pattern in the isolated rotor row seems to have little or no tendency to rotate.

As discussed earlier, the main difficulty with the Emmons model in transonic flow is that there is no 'unstalling' mechanism. Passage shock oscillation associated with shock-boundary layer interaction does, however, seem to provide a way to unstall. When an oscillating shock reaches its most upstream position, the separated vortical flow is shed downstream of the passage. If the stall is not too deep, the shed vortical flow can create sufficient change in blockage for either

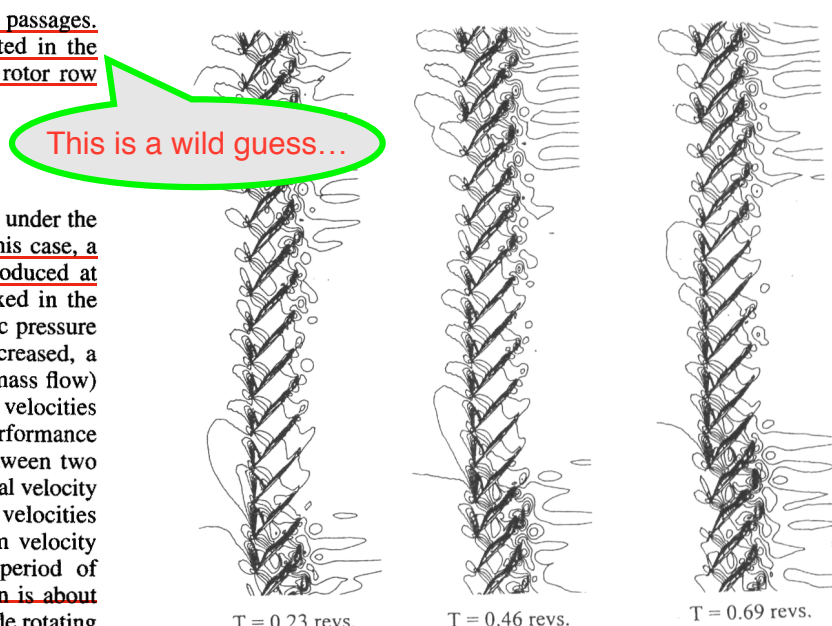


Figure 16. Mach number contours at four instants in one rotor revolution for an isolated rotor during stall inception.

the shock to move back into the passage or for a new shock to be formed. However, this unstalling mechanism cannot work once the passages become deeply stalled (Fig. 17).

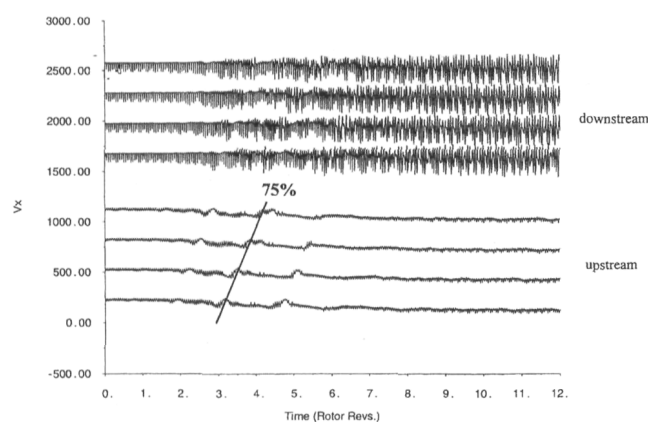


Figure 15. Time-history of axial velocity upstream and downstream of an isolated rotor during stall inception.

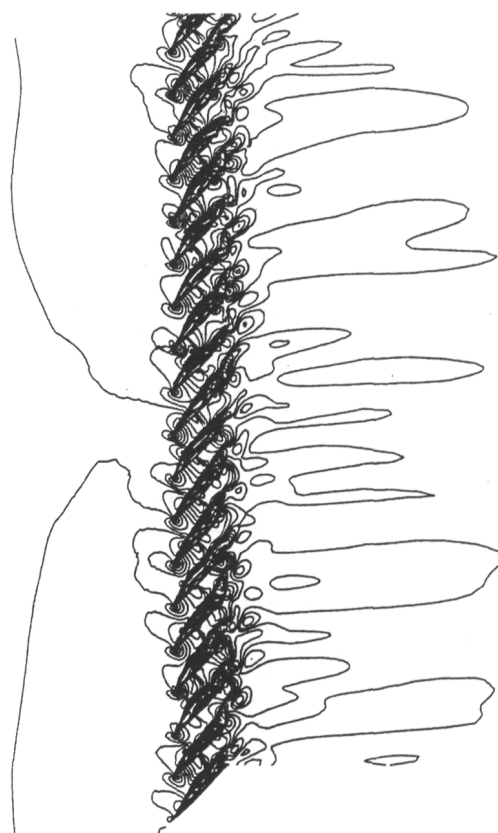


Figure 17. Instantaneous Mach number contours for an isolated rotor after stall inception.

## 6.0 CONCLUSIONS

The following conclusions can be drawn from the present computational study:

1. The mechanism for stall in blade rows under transonic conditions seems to be qualitatively different from that at subsonic conditions. For the NASA rotor-67, a part-span rotating stall was predicted at 50% speed. However, at 100% speed a one-dimensional breakdown of performance was predicted in which no rotating pattern could be clearly identified. This might be caused by the different circumferential information propagation upstream of a blade row at a supersonic condition compared that at a subsonic one.
2. During the stalling process at a transonic speed, there appears to be a strong interaction between tip leakage vortex and passage shock. In the prediction significant unsteadiness in the tip-clearance region was observed up to 20 revolutions before flow breakdown.
3. Two-dimensional computations illustrate that there might be two possible paths to rotating stall for a transonic rotor blade row. A rotor-stator stage calculation shows that a subsonic stator will go into rotating stall first and then force the stalled pattern in the rotor to rotate. For an isolated rotor row, self-excited oscillations of passage-shocks due to shock-boundary layer interaction may be circumferentially synchronised to generate a rotating pattern. However, this kind of rotating pattern was not observed in the present three-dimensional simulations for the NASA rotor-67.

## ACKNOWLEDGEMENTS

This work has been funded jointly by the Engineering and Physical Science Research Council of the UK and Rolls-Royce (GR/K16791). The authors wish to thank Dr P. Stow of Rolls-Royce for his continuing interest and technical support throughout this project.

## REFERENCES

1. DAY, I.J. Active suppression of rotating stall and surge in axial compressors, *ASME J Turbom.*, 1993, **115**, (1).
2. EPSTEIN, A.H., FFOWCS-WILLIAMS, J.E. and GREITZER, E.M. Active suppression of aerodynamic instabilities in turbomachines, *AIAA J Prop and Pow.*, 1989, **5**, (2).
3. MOORE, F.K. and GREITZER, E.M. A theory of post-stall transients in axial compressors: Part I — development of the equations, *ASME J Eng Gas Turb and Pow.*, 1986, **108**, pp 231-239.
4. GREITZER, E.M. Surge and rotating stall in axial flow compressors, *ASME J Eng Gas Turb and Pow.*, 1976, **98**, pp 190-217.
5. SISTO, F., WU, W., THANGAM, S. and JONNAVITHULA, S. Computational aerodynamics of oscillating cascade with evolution of rotating stall, *AIAA J*, 1989, **27**, (4), pp 462-471.
6. OUTA, E., KATO, D. and CHIBA, K. A N-S simulation of stall cell behaviour in a 2D compressor rotor-stator system at various loads, *ASME Paper*, 94-GT-257, 1994.
7. HE, L. Integration of 2D fluid/structure coupled system for calculations of turbomachinery aerodynamic/aeroelastic instabilities, *Int J CFD*, 1994, **3**, pp 217-231.
8. STRAZIAR, A.J. and POWELL, J.A. Laser anemometer measurements in a transonic axial flow compressor rotor, *ASME J Eng Pow.*, 1981, **103**, (2).
9. HUGHES, W.F. and BRIGHTON, J.A. *Fluid Dynamics*, 1967, Schaum's Outline Series, McGraw-Hill, New York.
10. BALDWIN, B.S. and LOMAX, H. Thin layer approximation and algebraic model for separated turbulent flows, *AIAA Paper* 78-0257, January 1978.
11. HE, L. and DENTON, J.D. Three-dimensional time-marching inviscid and viscous solutions for unsteady flows around vibrating blades, *ASME J Turbom.*, 1994, **116**.
12. GILES, M.B. Nonreflecting boundary conditions for Euler equation calculations, *AIAA J*, 1990, **28**, (12).
13. JAMESON, A., SCHMIDT, W. and TURKEL, E. 1981, Numerical solution of Euler equations by finite volume methods using Runge-Kutta time-stepping schemes, *AIAA Paper* 81-1259, 1981.
14. HE, L. New two-grid acceleration method for unsteady Navier-Stokes calculations, *AIAA J Prop and Pow.*, 1993, **9**, (2).
15. ARNONE, A. Viscous analysis of three-dimensional rotor flow using a multi-grid method, *ASME J Turbom.*, 1994, **116**, (1).
16. PUTERBAUGH, S.L. and BRENDL, M. Tip-clearance flow-shock interaction in a transonic compressor rotor, *AIAA J Prop and Pow.*, 1997, **13**, (1).
17. ISMAEL, J.O. and HE, L. Three-dimensional computation of rotating stall inception, 2nd European Conference on Turbomachinery, Antwerp, Belgium, March, 1997.
18. EMMONS, H.W., PEARSON, C.E. and GRANT, H.P. Compressor surge and stall propagation, *Trans ASME*, 1955, **77**, (4).
19. ADAMCZYK, J., CELESTINA, M.L. and GREITZER, E.M. The role of tip clearance in high speed fan stall, *ASME J Turbom.*, 1993, **115**.
20. HE, L. Computational study of rotating stall inception in axial compressors, *AIAA J Prop and Pow.*, 1997, **13**, (1).
21. DAY, I.J. Stall inception in axial flow compressors, *ASME J Turbom.*, 1993, **115**, January 1993, pp 1-9.